Supplementary Information for:

Generation and Control of Extreme-ultraviolet Spatiotemporal Skyrmions and Vector Hopfions with High Harmonic Generation

Jia-Hao Dong[1], **Liang Xu**[1,*], **Qing-Qing Liang**[1], **Ji-Jun Feng**[1,†], **Song-Lin Zhuang**[1], **and Yi Liu**[1,‡]

[1]Shanghai Key Lab of Modern Optical System, University of Shanghai for Science and Technology, Shanghai 200093, China

[*]E-mail: liangxu2021@usst.edu.cn

[†]E-mail: fjijun@usst.edu.cn

[‡]E-mail: yi.liu@usst.edu.cn

S1 Direction-mismatched two-color driving field

Here, we continue to adopt the expression $\mathbf{E}(\omega, q, m, \varphi_\gamma)$ used in the main text to describe a spatiotemporal skyrmion, where the parameters ω, q, m, and φ_γ represent its circular center frequency, polarity, vorticity, and the global phase difference between the Gaussian and spatiotemporal optical vortex (STOV) components, respectively. In this configuration, the fundamental wave (FW) at 800 nm, $\mathbf{E}(\omega_0, -1, -1, \pi/2)$, remains the same as that in the main text, as shown in Figs. S1a and b. However, the Stokes vector of the second harmonic (SH) at 400 nm, $\mathbf{E}(2\omega_0, 1, 1, \pi/2)$, in Fig. 1e in the main text is rotated around the s_3-axis (y-axis) by 180 degrees to obtain $\mathbf{E}(2\omega_0, 1, 1, -\pi/2)$, as illustrated in Fig. S1c. The projection of the Stokes vector of the FW and SH in the s_1-s_2 plane (ξ-x plane) is in opposite directions at any point (ξ, x), which indicates that the major-axis direction of the rotated SH is orthogonal to that of the FW, as shown in Figs. S1b and d. We refer to this laser-field configuration as the direction-mismatched two-color driving field. The resulting local trajectories of the electric vector of this synthetic two-color field are typical Lissajous curves, as illustrated in Fig. S1e. The orthogonal major axes rotate the electric vector alternately clockwise and counterclockwise, causing the instantaneous spin angular momentum (SAM) density to periodically change its sign at the oscillation frequency of the FW[1], as shown in Fig. S1f.

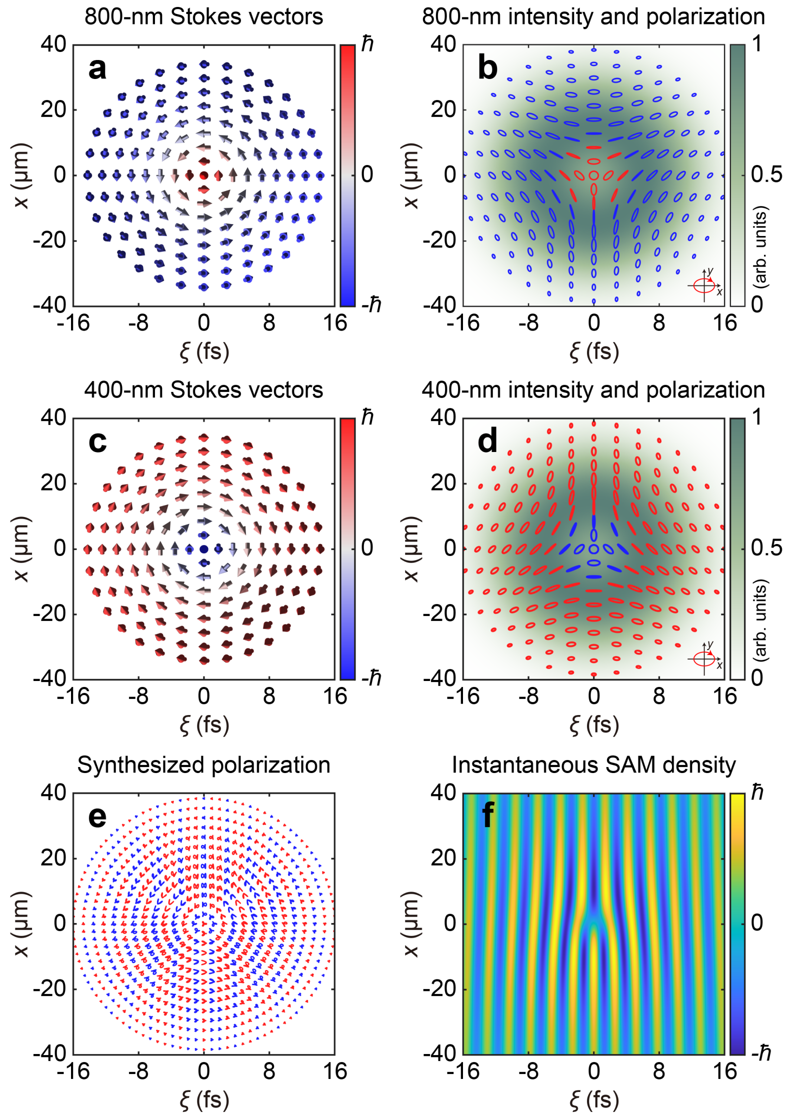

Figure S1. **Schematic diagram of the direction-mismatched two-color driving field. a-d** Spatiotemporal distributions of normalized Stokes vectors $\mathbf{s} = (s_1, s_2, s_3)$, normalized total intensity, and polarization for the 800-nm and 400-nm spatiotemporal skyrmions, where the red (blue) arrows and curves mean that the spin direction of the local field corresponds to a right-handed (left-handed) rotation. **e** The local trajectories of the electric vector of the synthetic field. **f** Spatiotemporal distributions of the instantaneous SAM density of the synthetic field.

As discussed above, an orthogonal two-color field introduces additional SAM density in addition to the intrinsic SAM associated with the polarization of the laser field. When the intrinsic SAM of the FW and SH completely cancel each other, the SAM density only arises from the orthogonal major axes, independent of the circular polarization directions of the two fields. The spatiotemporal spiral phase difference between the STOV and Gaussian components causes the polarization ellipse to rotate around the center point ($\rho = 0$). Although the rotation direction remains consistent along any ring with radius ρ, it differs across cross-sections at different x positions.

As shown in Fig. S1b, for $x > 0$, the polarization ellipse rotates counterclockwise over time ξ, which is opposite to the clockwise rotation of the FW electric vector, thus slowing the oscillation of the FW field. In contrast, for $x < 0$, the polarization ellipse rotates clockwise over time, accelerating the oscillation of the FW field. At $x = 0$, the major-axis direction of the polarization ellipse remains nearly time-invariant, except for an abrupt change in 45° when crossing the center point ($\rho = 0$), which results from the phase singularity of the STOV component.

Consequently, compared to $x > 0$, the FW field experiences an additional oscillation cycle for $x < 0$. Combined with the aforementioned periodic variation of the instantaneous SAM density at the FW frequency, the composite field exhibits a fork-shaped instantaneous SAM distribution with a fork number of one, as illustrated in Fig. S1f.

S2 Harmonics produced by direction-mismatched two-color driving fields

Figure S2 presents the characteristics of the 13th harmonic generated by the direction-mismatched two-color driving field as mentioned in Fig. S1. The complex additional SAM density of this driving field severely disturbs the SAM conservation during the HHG process and muddles the polarization structure of the harmonics, as shown in Figs. S2a and b. Thus, our probability estimation method proposed in the main text is no longer applicable, as indicated by the green and purple dotted lines in Fig. S2c.

Note that the degree of influence of the direction mismatch depends on the angle between the main axes of the two-color driving field (data not shown). When the main axes of the FW and SH are parallel, no additional SAM density arises, enabling the generation of well-defined spatiotemporal skyrmionic harmonics, as discussed in the main text. As the angle between the two increases, the effect of direction mismatch becomes more pronounced and reaches its maximum when the two axes are orthogonal. In this case, the harmonic mode exhibits the highest degree of disorder.

In summary, the spin-orbit coupling effect in the interaction between structured fields and matter ensures that the topological properties of the driving field can be coherently transferred to the harmonics, which originates from SAM conservation. When the Stokes vectors of the two-color driving fields are matched (i.e., the polarization-ellipse major axes are parallel), the contributions of the FW and SH fields to the SAM of the harmonic photons are well defined. However, when the Stokes vectors of the two-color

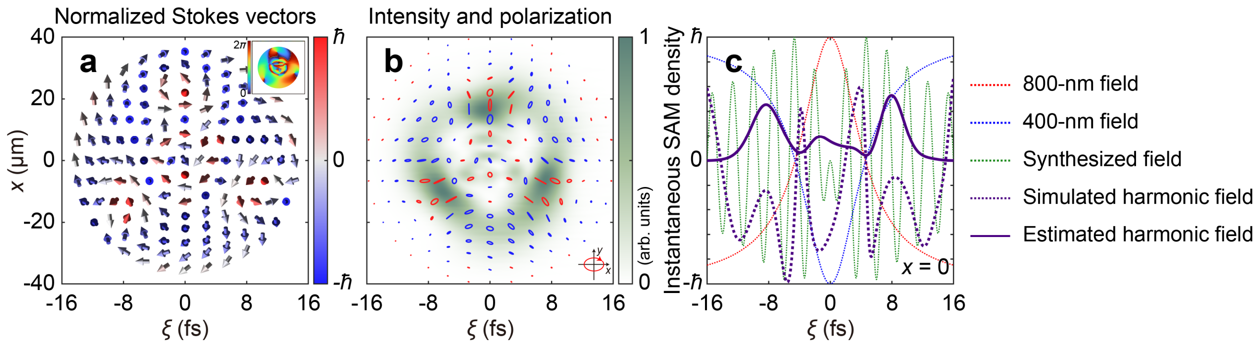

Figure S2. Harmonic structure driven by the direction-mismatched two-color driving field. a-b, Spatiotemporal distributions of normalized Stokes vectors $\mathbf{s} = (s_1, s_2, s_3)$, normalized total intensity, and polarization for the 13th harmonic. In the inset of **a**, the spatiotemporal distribution of the orientation of the polarization-ellipse major axis is shown. **c** Instantaneous SAM density of the driving field and the 13th harmonic for $x = 0$.

fields are mismatched (i.e., the polarization-ellipse major axes are orthogonal), the coupling between the FW and SH fields introduces additional time-varying SAM density. However, this SAM originates from the field configuration itself. Although we can calculate the instantaneous SAM density of the synthesized field, we cannot distinguish the contributions of the instantaneous SAM density absorbed during harmonic photon emission. This represents a limitation of the photon absorption model we proposed.

S3 3D structure of the vector hopfion

Here, we take the 800-nm driving field — composed of a vortex pulse ($\ell_z = 1$) with a right-hand circular polarization (RCP) and a toroidal vortex pulse ($\ell_\perp = 1$) with a left-hand circular polarization (LCP), as described in the main text — as an example to illustrate the three-dimensional structure of the vector hopfion. The spiral phase structure of the vortex beam in the x–y plane provides a continuously varying global phase difference with respect to the azimuthal angle $\varphi_z = \tan^{-1}(y/x)$ for the two components with opposite spins, giving rise to the distinctive Hopf-fibre topology of the hopfion, as illustrated in Fig. S3a. Hopf fibres in a hopfion are a family of closed curves, forming a nontrivial 3D linkage characterized by the Hopf invariant[2]:

$$Q_H = Q_P \times Q_V \tag{S1}$$

where polarity Q_P and vorticity Q_V are defined by the Stokes vector distribution. For $Q_P = 1$ ($Q_P = -1$), under the topological mapping $(s_1, s_2, s_3) \leftrightarrow (z, x, y)$, the Stokes vector points in the negative (positive)

y-direction at $r = 0$, and in the positive (negative) y-direction at $r = r_0$. The vorticity depends on the skyrmion number of the laser field within the longitudinal cross-section (x–y) at $z = 0$. A Hopf fibre indicates that every point of the hopfion along this trajectory possesses exactly the same Stokes vector and polarization state, as shown in Fig. S3b.

A cross-section obtained by slicing the hopfion along an arbitrary diameter contains two skyrmions with opposite skyrmion numbers (both exhibit right-handed circular polarization at their centers, $r = r_0$, but their Stokes vectors rotate in opposite directions), as shown in Fig. S3c. This arises because at two diametrically opposite points of the ring, the spatial vector $\mathbf{r}$ points in opposite directions, giving rise to a pair of skyrmionic enantiomers.

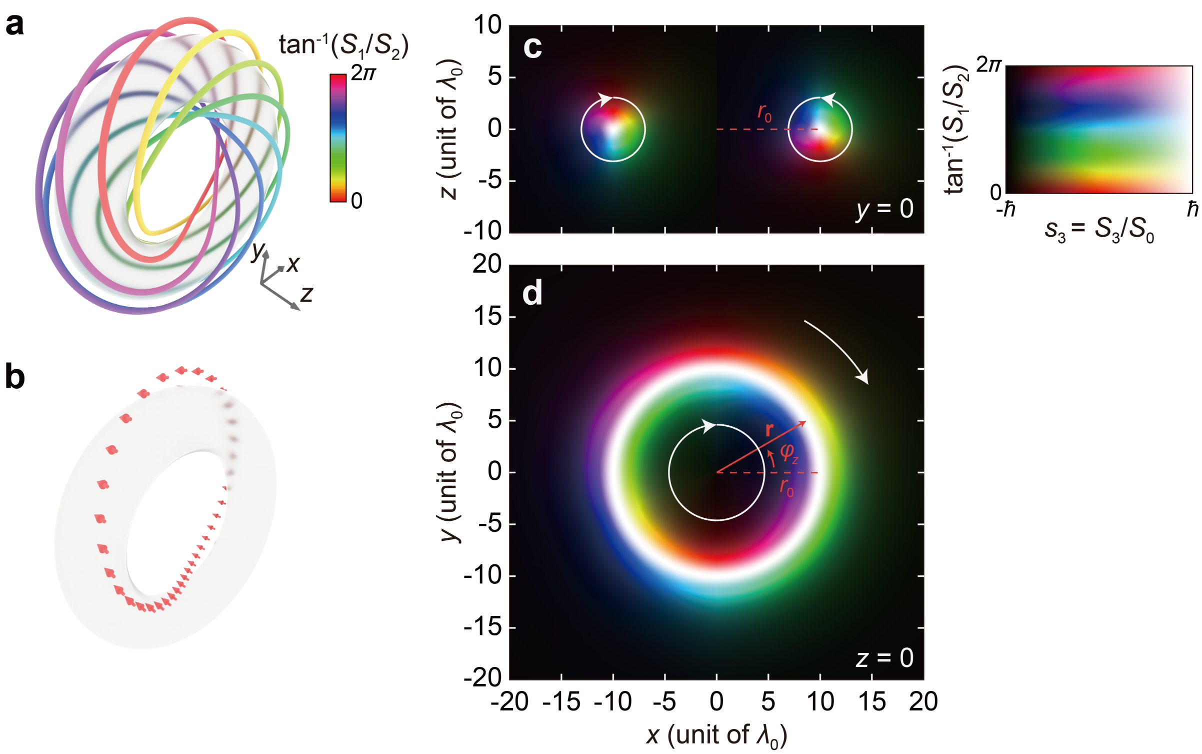

Figure S3. Schematic diagram of the 800-nm vector hopfion. a Structural diagram of Hopf fibres. **b** Each color of Hopf fibres represents a Stokes vector or a direction of the major axis of the polarization ellipses. **c-d** Polarization distributions of the 800-nm vector hopfion in the x-z plane (**c**) and the x-y plane (**d**). For a pure color, a lighter shade indicates that the polarization at that point is closer to the RCP, while a darker shade suggests it is closer to the LCP.

In the longitudinal cross-section at $z = 0$, the Stokes vector exhibits a skyrmionium structure with a bilayer ring configuration, where the inner and outer rings possess opposite polarities, as shown in Fig.

S3d. The black region at the center ($r = 0$) corresponds to the LCP, indicating that the Stokes vector points along the negative y-direction. At $r = r_0$, the white circular ring corresponds to the RCP, with the Stokes vector at the boundary of the inner skyrmion pointing along the positive y-direction. This confirms that the 800-nm vector hopfion has a polarity of $Q_P = 1$. Furthermore, the Stokes vector of the inner skyrmion rotates clockwise in the x–y plane, opposite to the anticlockwise increasing direction of φ_z, indicating that the inner skyrmion is an anti-skyrmion and therefore corresponds to $Q_V = -1$. According to Eq. S1, the Hopf invariant of the 800-nm vector hopfion is thus $Q_H = -1$. Similarly, for the 400-nm vector Hopfion consisted of an LCP vortex pulse ($\ell_z = -1$) and an RCP toroidal vortex pulse ($\ell_\perp = -1$), the topological parameters $Q_P = -1$ and $Q_V = -1$, leading to a Hopf invariant of $Q_H = 1$, as shown in Fig. S4. Note that by comparing Figs. S3 and S4, it can be observed that the major-axis directions of the polarization ellipses for the 800-nm and 400-nm vector Hopfions are exactly the same. Therefore, the synthesized field is a direction-matched two-color driving field.

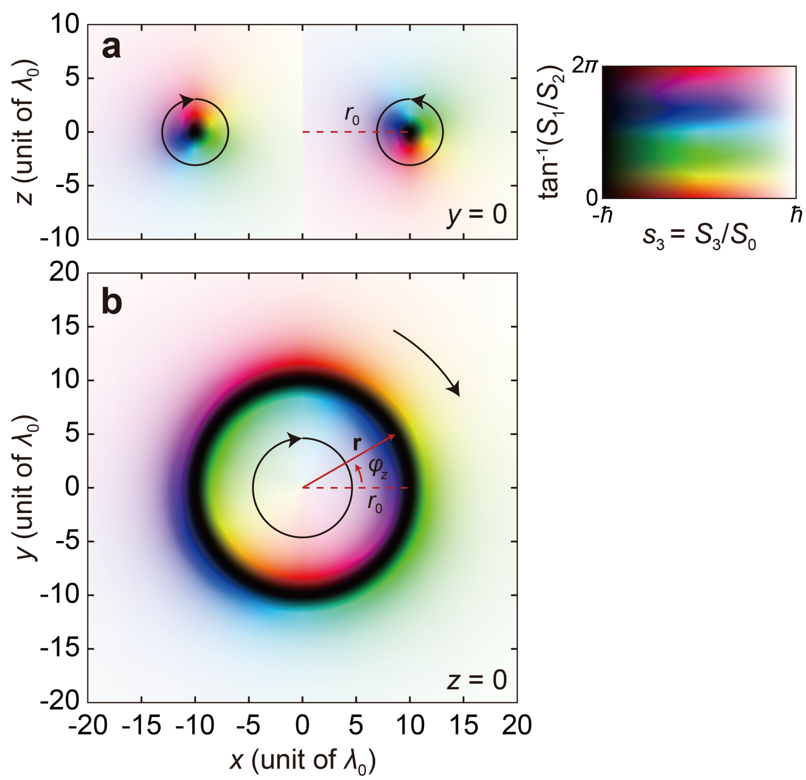

Figure S4. **Schematic diagram of the 400-nm vector hopfion. a-b** Same as the illustration in Fig. S3c-d, but these results are calculated for the 400-nm driving field.

References

1. Fang YQ, Liu YQ. Optimal control over high-order-harmonic ellipticity in two-color cross-linearly-polarized laser fields. Phys. Rev. A 2021;103:033116.

2. Shen YJ, Yu BS, Wu HJ, Li CY, Zhu ZH, Zayats AV. Topological transformation and free-space transport of photonic hopfions. Adv. Photonics 2023;5:015001.